

## APPLICATION OF TWO-STEP DIFFUSION COUPLE TECHNIQUE IN HIGH-THROUGHPUT SCREENING OF OPTIMAL COMPOSITION AND AGING TEMPERATURES FOR ALLOYS DESIGN: A DEMONSTRATION IN BINARY Ni-AL SYSTEM

Y.-J. Shang<sup>b</sup>, D.-J. Cao<sup>b</sup>, Q. Li<sup>b,\*</sup>, K. Yang<sup>a</sup>, C.-M. Deng<sup>a</sup>, L.-J. Zhang<sup>a,b,#</sup>

<sup>a</sup> Institute of New Materials, Guangdong Academy of Sciences,  
National Engineering Laboratory for Modern Materials Surface Engineering Technology,  
The key Lab of Guangdong for Modern Surface Engineering Technology, Guangzhou, China  
<sup>b</sup> State Key Laboratory of Powder Metallurgy, Central South University, Changsha, Hunan, China

(Received 23 December 2019; Accepted 19 January 2021)

### Abstract

In this paper, four binary Ni-13.4 at.% Al/Ni-17.7 at.% Al diffusion couples were first prepared and subjected to homogenization at 1573 K for 10,800 s, from which a continuous concentration profile formed. The three diffusion couples were then cooled down for aging at respective temperatures, i.e., 1173, 1123, and 1073 K, for 14400 s. The effect of composition and aging temperature on the aging microstructure was studied in detail by means of different experimental techniques and statistical analysis. The volume fraction, grain size, and shape factor of  $\gamma'$  precipitates in the three diffusion couples were plotted as a function of alloy composition and annealing temperatures. Together with the previously proposed evaluation function in which the phase fraction, grain size, and shape factor of  $\gamma'$  precipitates were chosen as the evaluation indicators, the optimal alloy composition and aging temperature for binary Ni-Al alloys with the best mechanical properties were evaluated, and finally validated by the measured hardness values. The successful demonstration of alloy design in the present binary Ni-Al alloys indicated that the two-step diffusion couple, together with the evaluation function for mechanic properties, should be of generality for high-throughput screening of optimal alloy composition and heat treatment process in different alloys.

**Keywords:** Two-step diffusion couple; Ni-Al alloys; Microstructure; Hardness; Alloys design

### 1. Introduction

Ni-based superalloys, mainly consisting of chemically disordered  $\gamma$  matrix and chemically ordered  $\gamma'$  precipitates, are widely used as engine blades and turbine discs in aerospace fields because of their excellent mechanical performance at high temperatures [1-4]. The performances of alloys are closely related to their microstructures, such as volume fraction, grain size, and morphology of the  $\gamma'$  precipitates, which strongly depend on alloy composition and heat-treatment processes. Therefore, a large number of experiments have been devoted to studying the effects of alloy composition and heat treatment process on the microstructure and properties of Ni-based superalloys [5-12] in order to improve the high-temperature strength and creep resistance of Ni-based superalloys. Qiu [8] observed the anomalous coarsening behavior of  $\gamma'$  precipitates in Ni-based

superalloys after aging process. Nathal [9] investigated the influence of size and shape of  $\gamma'$  grains on the high temperature creep properties of Ni-based superalloys. Ges et al. [10] studied the effect of heat treatments on the  $\gamma'$  precipitate sizes and distribution in a CMSX-2 superalloy. Besides, the influence of Al content on the microstructure and creep behavior of Ni-based superalloy was also investigated by Fu et al. [11]. However, significant disadvantages exist in the traditional 'trial-and-error' method because of its low efficiency, and time/money-consuming process. Thus, the theoretical investigations may serve the supplement. In fact, there also exist certain amounts of modeling work on the microstructure evolution of Ni-based superalloys during different processes using, for instance, the powerful phase-field simulations [13-17]. Though the theoretical modeling can save time and money, its reliability should be validated by key experiments.

Corresponding author: qinli333@csu.edu.cn \*; lijun.zhang@csu.edu.cn #;



In recent years, the Materials Genome Initiative (MGI) project has promoted the emergence of various high-throughput technologies [18] in combination with micrometer-scale property measurement tools, which can accelerate the study on the properties of alloys, such as thermal conductivity, diffusivity, hardness, and elastic modulus, and so on [19, 20]. In the spirit of MGI, a series of methods utilizing the macro-component gradient of samples have been originally proposed to determine the phase diagrams at relatively low temperatures [21, 22], to evaluate the interfacial energy [23-25], and recently employed to obtain the abundant information on microstructure and different properties within the specified alloy composition range in a high-throughput way. One of such methods is the so-called two-step diffusion couple technique [19, 26, 27]. Taking the binary Ni-Al system for example, the sample preparation of a two-step diffusion couple can be illustrated in Fig. 1: (i) two single-phase alloys with different compositions ( $x_A$  and  $x_B$ ) are combined together and annealed at a high temperature (i.e.,  $T_1$ , at which both alloys with composition  $x_A$  and  $x_B$  locate in the single-phase region) for a certain period to obtain a continuous composition region; and (ii) the diffusion couple is then cooled down from  $T_1$  to a relatively lower temperature (i.e.,  $T_2$ , at which precipitates appear in the single-phase diffusion couple) and annealed for certain time to obtain the microstructure of the continuous composition at  $T_2$ . Only at this point can a two-step diffusion couple be prepared successfully.

Furthermore, the two-step diffusion couple technique in combination with different micrometer-scale property measurement tools can improve the screening efficiency of the alloy composition and the heat treatment process with optimum properties.

Consequently, the Ni-Al binary system is taken as the target in this paper. Three Ni-Al two-step diffusion couples are to be prepared, and the continuous composition-dependent microstructure forming during annealing at three different temperatures will be measured. After that, the optimal alloy composition and aging temperature corresponding to the optimal mechanical properties for binary Ni-Al alloys can be then screened efficiently based on the previously proposed property evaluation function [15] together with the measured microstructure information. Finally, the screened alloy composition and aging temperature with the optimal mechanical property are validated by the experimentally measured hardness in the three diffusion couples.

## 2. Experimental procedure

Ni-13.4 at.% Al and Ni-17.7 at.% Al alloy ingots were prepared in an argon atmosphere by using an arc-melting furnace (WKDHL-1, Optoelectronics Co., Ltd., Beijing, China). Ni ingots (purity: 99.99 wt.%) and Al pieces (purity: 99.99 wt.%) were used as the raw materials. Subsequently, the Ni-13.4 at.% Al and Ni-17.7 at.% Al alloy ingots were cut into blocks approximately 5 mm×5 mm×2.5 mm in size and

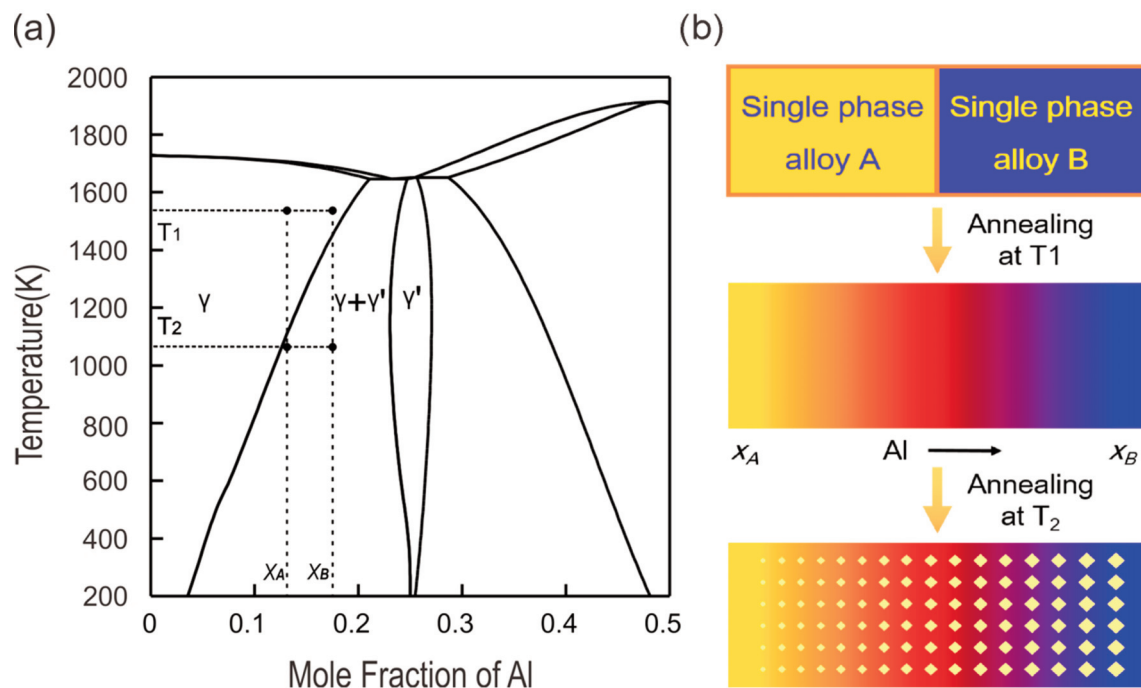


Figure 1. (a) Ni-rich Ni-Al phase diagram; (b) Schematic diagram for preparation of a two-step diffusion couple

annealed in vacuum-sealed quartz tubes at  $1573 \pm 3$  K for 18000 s (5 hours) in a high-temperature diffusion furnace (GSL1700X, Hefei Kejing Materials Technology Co., Ltd., Hefei, China) to improve their homogeneity. All the homogenized alloys were subjected to X-ray diffraction detection (XRD, D8 Advance, Bruker, Germany) to confirm that only the  $\gamma$  phase existed in these samples. As shown in Fig. 2, the XRD patterns suggested that the two alloys were located in the single  $\gamma$  phase region. After being polished and cleaned, the polished surfaces of the alloys were stuck together and then bound together to prepare diffusion couples by using two pieces of Mo plates, which were fastened by screws. Four Ni-13.4 at.% Al/Ni-17.7 at.% Al diffusion couples were annealed at  $1573 \pm 3$  K for 10800 s (3 hours) in vacuum sealed quartz tubes to form the continuous composition profiles. After that, one of four diffusion couples was taken out and quenched in water, and then its concentration profile was measured by means of electron probe microanalysis (EPMA, JXA-8230, JEOL, Japan). Meanwhile, the other three diffusion couples were cooled to  $1073 \pm 3$  K,  $1123 \pm 3$  K, and  $1173 \pm 3$  K at a rate of  $10 \text{ K min}^{-1}$  respectively in the high-temperature diffusion furnace and then aged for 14400 s (4 hours), followed by water quenching.

The microstructure and hardness of the three diffusion couples after aging at 1073, 1123, and 1173 K for 14400 s were tested by different techniques: the microstructure along diffusion paths was characterized using scanning electron microscopy

(SEM); then, the grain size and the volume fraction of the  $\gamma'$  phase in SEM images were measured by Image-Pro plus 6.0 metallographic analyzer. Later, the Vickers hardness of the three two-step diffusion couples was determined by nanoindentation (NHT2, Anton Paar, Austria). The nanoindentation tests were performed with the maximum indentation load of 20 mN, loading rate of  $40 \text{ mN min}^{-1}$ , and loading time of 10 s in the maximum loading, and the hardness was measured every  $100 \mu\text{m}$  along diffusion paths of the diffusion couples. Each point was tested 3 times, and the mean value was accepted.

### 3. Results and discussion

#### 3.1. Experimental results

The measured Al concentration profile of the Ni-Al diffusion couple annealed at 1573 K for 10800 s is displayed in Fig. 3 (denoted in red symbol). The model-predicted composition profile (denoted in curve), according to Zhang et al. [28], was also superimposed for a comparison. As can be seen, the model-predicted composition profile was in excellent agreement with the present experimental data. According to Zhao [23] and Miyazaki [25], the effect of aging treatments at lower temperatures (i.e., 1073, 1123, and 1173 K) on the composition gradient created during the higher temperature annealing (1573 K) can be neglected. This is because: (i) the difference between the diffusing and aging temperatures was over 400 K, which resulted in the diffusion coefficient

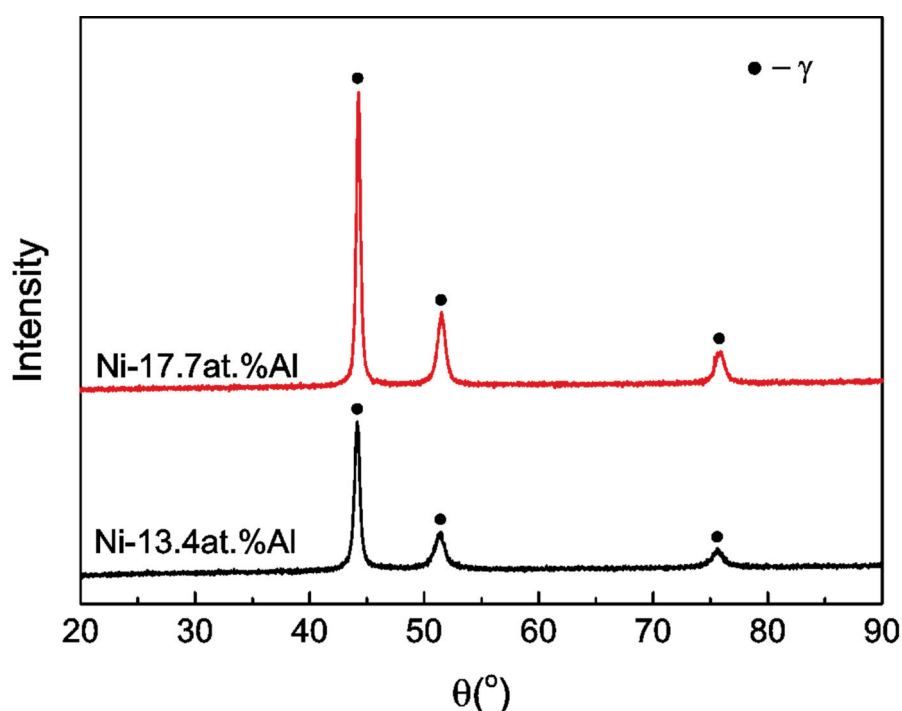
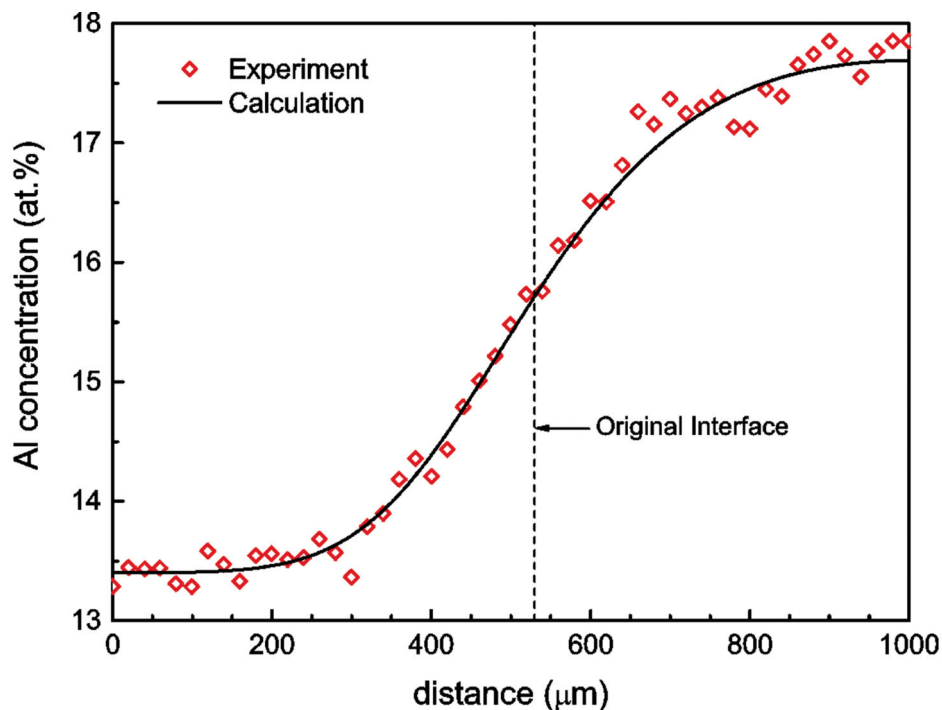


Figure 2. X-ray diffraction patterns of Ni-13.4 at.% Al and Ni-17.7 at.% Al alloys after annealing at 1573 K for 18000 s

of solute atoms at diffusing temperature was larger than that at the aging temperature by  $10^3$  times [28, 29]; (ii) the aging time (14400 s in this work) was too short for the composition profile to change as a function of distance at lower temperatures; and (iii) compared with the chemical driving force for the formation of  $\gamma'$ , the driving force for interdiffusion was too small. Therefore, it can be assumed that the average composition profile of the two-step diffusion couples was the same as that of the diffusion couple only annealed at 1573 K. Moreover, the microstructure of the Ni-13.4 at.% Al/Ni-17.4 at.% Al diffusion couples aging at 1073 K, 1123 K, and 1173 K are shown in Fig. 4. It can be seen that both the size and volume fraction of  $\gamma'$  precipitates increased as Al content increased, which can be attributed to that as Al content increased, (i) the equilibrium fraction of  $\gamma'$  precipitates increased according to the level rule of the Ni-Al phase diagram (see Fig. 1), and (ii) the driving force for the formation of  $\gamma'$  precipitates [30] and the interdiffusion coefficients of the  $\gamma$  matrix [28] both increased.

Moreover, it also can be observed that with the increase of Al content and the growth of precipitates from left side to right side of Fig. 4, the small square  $\gamma'$  precipitates (cube in 3-D) gradually changed into the composed square (octocube in 3-D)/butterfly shape (octodendrites in 3-D crystals), and then to irregular shape. This change in morphology should

be attributed to the competition between the elastic strain energy associated with the lattice mismatch between  $\gamma$  and  $\gamma'$  phases and the interface energy [31-33]. During the evolution of  $\gamma'$  precipitates, at the initial stage, the shape of precipitates tended to be spherical since the contribution of interface energy was predominant when the precipitates were very small. Subsequently, the elastic contribution increased as the precipitates grew, and the shape of precipitates transformed into the cubic one since the elastic strain energy in an octagonal cube should be lower than that in a cube. Since the elastic strain energy in an octagonal cube should be lower than that in a cube [32, 34], the decrease of elastic energy was higher than the increase of interface energy caused by splitting when the precipitates exceeded a critical size, and the cubic precipitates thus split into octocube. Then, the further growth of the precipitates led to the formation of octo-dendrites. While with the increase of  $\gamma'$  phase volume fraction, the elastic interaction between precipitates increased dramatically, it resulted in a decrease of the driving force for splitting [34]. It has been found that cubic  $\gamma'$  phase was the required structure of Ni-based superalloy since it was stable during service life and could better prevent dislocation migration during the creep stage because of its larger lattice misfit [35, 36]. Moreover, a preferred orientation of  $\gamma'$  phase could be usually observed in superalloys,



**Figure 3.** Measured Al concentration profile of the Ni-13.4 at.% Al/Ni-17.7 at.% Al diffusion couple annealed at 1573 K for 10800s (denoted in red hollow diamond), compared with the model-predicted results by Zhang et al. [28] (denoted in black solid line)

but it was not apparent in this work. That may be due to the difference in heat treatment. In this work, after homogenization, the samples were cooled at a low rate (i.e., 10 K min<sup>-1</sup>). Such a low cooling rate could cause a low nucleus density, and the interaction among  $\gamma'$  phases could be neglected in the early stage of precipitating. Besides, the relatively high aging temperatures (1173 K, 1123 K, and 1073 K) and the short aging time (i.e., 4h in this work) also led to the random arrangement of  $\gamma'$  precipitates. Furthermore, the shape factor  $\zeta$  could be used to describe the geometric shape of the  $\gamma'$  precipitates [37]:

$$\zeta = \frac{4\pi A}{P^2} \quad (3-1)$$

where  $P$  is the perimeter of  $\gamma'$  precipitates and  $A$  is the area of  $\gamma'$  precipitates measured by the quantitative image analyzer. In this work, all the values of the calculated shape factor were below 0.785. In Equation (3-1), the closer to 0.785 the shape factor was, the closer to cube the shape was, and the closer to 0 the shape factor of irregular shape precipitation was. The evaluated shape factors according to the experimental data (denoted in solid spheres) are presented in Fig. 5. Moreover, the fitted results (denoted in solid lines) corresponding to each set of experimental data were also superimposed in the figure. Fig. 5 shows that the increase of the aging temperature decreased the shape factor. This was because the increase of the temperature led to the decrease of mismatch between the  $\gamma$  phase and  $\gamma'$  phase [38], and thus the cubic degree of the

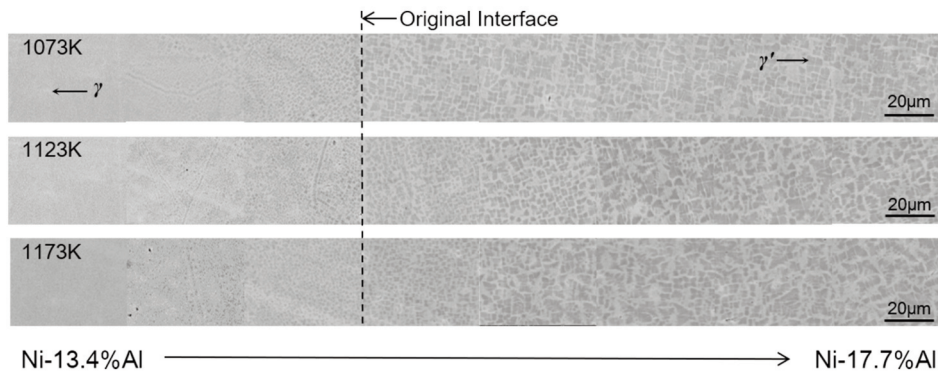


Figure 4. Backscatter electron images of the Ni-13.4 at. % Al/Ni-17.4 at. % Al diffusion couples after aging at 1073 K, 1123 K and 1173 K for 14400 s

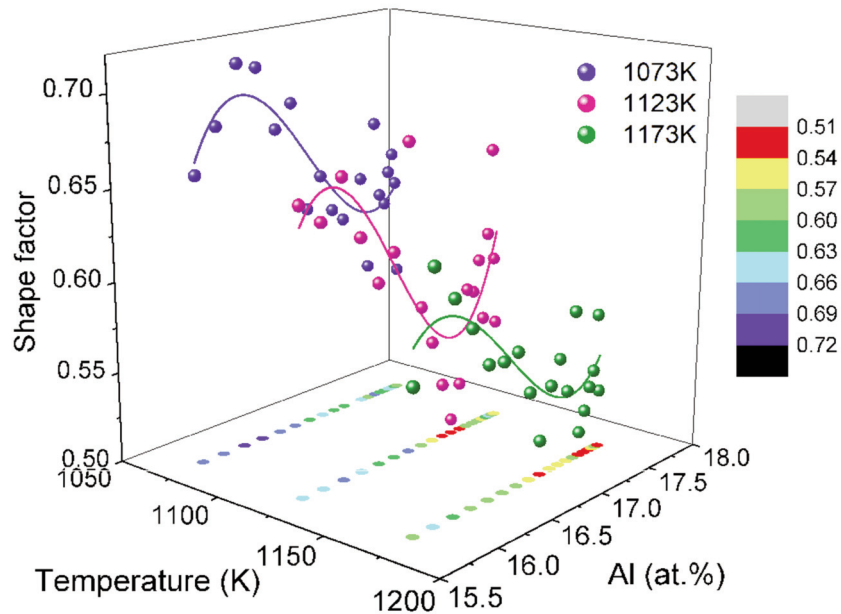


Figure 5. Evolution of shape factors of  $\gamma'$  precipitates evaluated from the experiment microstructures (denoted in solid spheres) as a function of Al composition and aging temperature, together with the fitted results using polynomial functions (denoted in solid lines)



morphology of  $\gamma'$  precipitates was reduced. Meanwhile, as the Al content increased, the shape factor increased and reached the maximum value (0.71) at around Ni-16 at.% Al. Subsequently, it decreased to the minimum and then increased slightly, which corresponded to the change in shape described above.

The relationship among the size of  $\gamma'$  precipitates, the aging temperature, and Al content is shown in Fig. 6. The variation of  $\gamma'$  precipitate size with the Al composition for each temperature was fitted, and the results (denoted in solid lines) were also added in Fig. 6. Since the shape of  $\gamma'$  precipitates was irregular (as shown in Fig. 4), it was difficult to obtain the size of  $\gamma'$  precipitates by measuring the diameter along a certain direction. Therefore, the shape of the precipitated phase was assumed to be circular with almost the same area to gain an average diameter, which could be calculated by the following expression [31]:

$$\bar{d} = \left( \frac{4A}{\pi} \right)^{0.5} \quad (3-2)$$

The average diameter of each  $\gamma'$  precipitate was calculated, and the mean value of these  $\gamma'$  precipitates was then obtained. The error bars represented the standard deviation from the mean value. It can be seen in Fig. 6 that the average size of  $\gamma'$  precipitates increased with the increase of the aging temperature, while it increased as the Al content increased at first and then it reached the maximum value, which was because the growth of  $\gamma'$  precipitates depended on the transport of

the solute. The diffusivities increased with the increase of temperature and also the increase of Al content, and the large diffusivities stimulated the growth of precipitates, which was controlled by diffusion. According to Refs. [39-41], the larger the grain size of  $\gamma'$  precipitates, the lower the strength of alloys.

Fig. 7 displays the volume fraction of  $\gamma'$  precipitates, and the error bars represented the standard deviation from the mean value of the volume fraction. The variation of the volume fraction of  $\gamma'$  precipitates with Al composition for each temperature was fitted, and the results (denoted in solid lines) were added in Fig. 7. Since the SEM results are typically two-dimensional images, one cannot directly obtain the volume fraction of  $\gamma'$  phases. Therefore, the following expression was utilized to evaluate the volume fraction [42]:

$$f_V = \frac{\pi}{6} N_A \bar{d}^2 \quad (3-3)$$

where  $\bar{d}$  is average  $\gamma'$  precipitates diameter and  $N_A$  is particle density. As can be seen in Fig. 7, the volume fraction of  $\gamma'$  precipitates increased almost linearly with the increase of Al content, while it slightly decreased as the aging temperature increased, which conformed to the lever rule. According to the lever rule in binary alloys, the equilibrium phase fraction can be calculated based on the Ni-Al phase diagram (Fig.1 (a)), in which the volume fraction of  $\gamma'$  precipitates is proportional to Al content and increases when the temperature decreases.

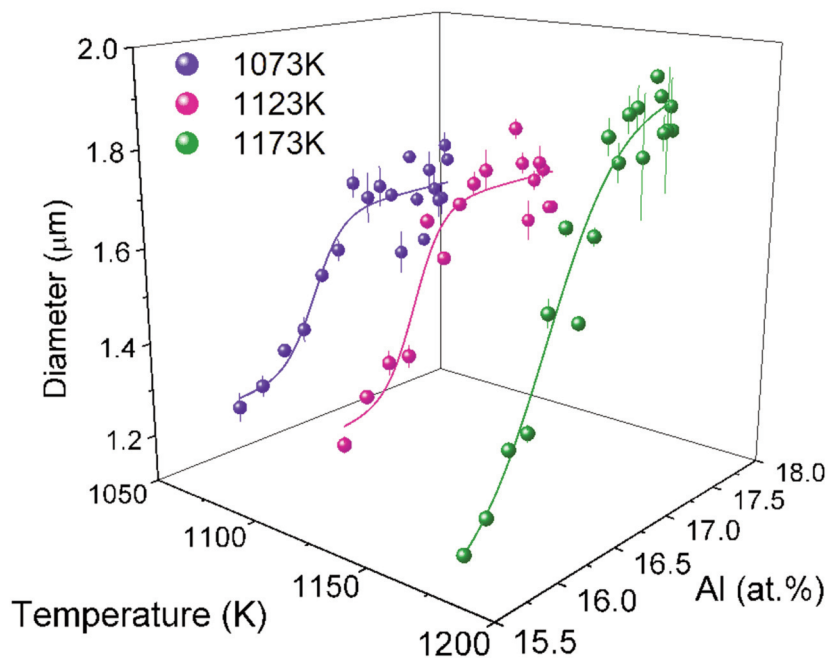


**Figure 6.** Evolution of diameter of  $\gamma'$  particles evaluated from the experiment microstructures (denoted in solid spheres) as a function of Al composition and aging temperature, together with the fitted results using polynomial functions (denoted in solid lines)

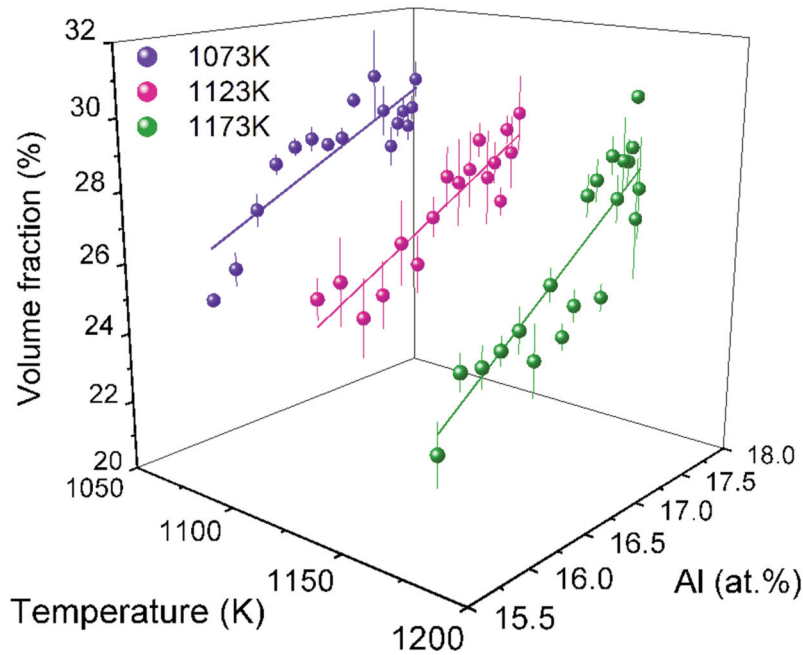


**Figure 7.** Evolution of volume fractions of  $\gamma'$  precipitates evaluated from the experiment microstructures (denoted in solid spheres) as a function of Al composition and aging temperature, together with the fitted results using polynomial functions (denoted in solid lines)

### 3.2. Evaluation of optimal alloys composition/aging temperature and its validation

As mentioned above, the mechanical properties of Ni-based alloys strongly depended on the microstructure of the material, including the volume fraction, grain size, and geometric shape of  $\gamma'$  precipitates. Therefore, based on the concept of Fuzzy Mathematics, a composite indicator, in which volume fraction, grain size, and shape factor of  $\gamma'$  precipitates were chosen as evaluation indicators, was proposed in our research group [15] to evaluate the optimal alloy composition and aging process. The composite indicator was established by assigning empowered weights  $w_1$ ,  $w_2$ , and  $w_3$ , for the different indicators,

$$\text{Composite Indicator} = w_1 \times f_v - w_2 \times \bar{d} + w_3 \times \xi \quad (3-4)$$

where the composite indicator increased with the increase of volume fraction  $f_v$  and shape factor  $\xi$ , while it decreased with the increase of diameter  $\bar{d}$ . With the maximum value of "Composite Indicator", a point that balances the three indicators at the best degree was achieved. The empowered weights  $w_1$ ,  $w_2$ , and  $w_3$  were calculated by the following equations:

$$w_i = \frac{w_i^*}{\sum_n w_i^*} \quad (3-5)$$

$$w_i^* = \sin(\text{Indicator membership}) \quad (3-6)$$

$$\text{Indicator membership} = \frac{\text{Indicator} - \text{Indicator}_{\min}}{\text{Indicator}_{\max} - \text{Indicator}_{\min}} \quad (3-7)$$

where "Indicator" represents volume fraction, grain size, and shape factor.

The composite indicator of the present experimental data is shown in Fig. 8. The alloy composition and the aging temperature corresponding to the maximum value of the composite indicator (0.295) were Ni-16.2 at.% Al alloy and 1073 K, at which the optimal mechanical property were achieved in Ni-16.2 at.% Al aging at 1073 K.

Furthermore, the measured hardness of the three two-step diffusion couples is shown in Fig. 9. The hardness of alloys decreased as the aging temperature increased. Meanwhile, it increased first as the increase of Al content and reached the maximum value at the composition around Ni-16.2 at.% Al. Then, the hardness decreased as the Al content increased. That was probably because of the increase of  $\gamma'$  phase size. The alloy with the highest hardness was Ni-16.2 at.% Al, and the aging temperature was 1073 K, which was consistent with the result predicted by the linear synthesizing evaluation function. The successful prediction of the alloy composition and heat treatment process for binary Ni-Al alloys with optimal mechanical properties indicated that the two-step diffusion couple technique can be used for high-throughput screening of optimal composition and aging temperatures for alloy design.

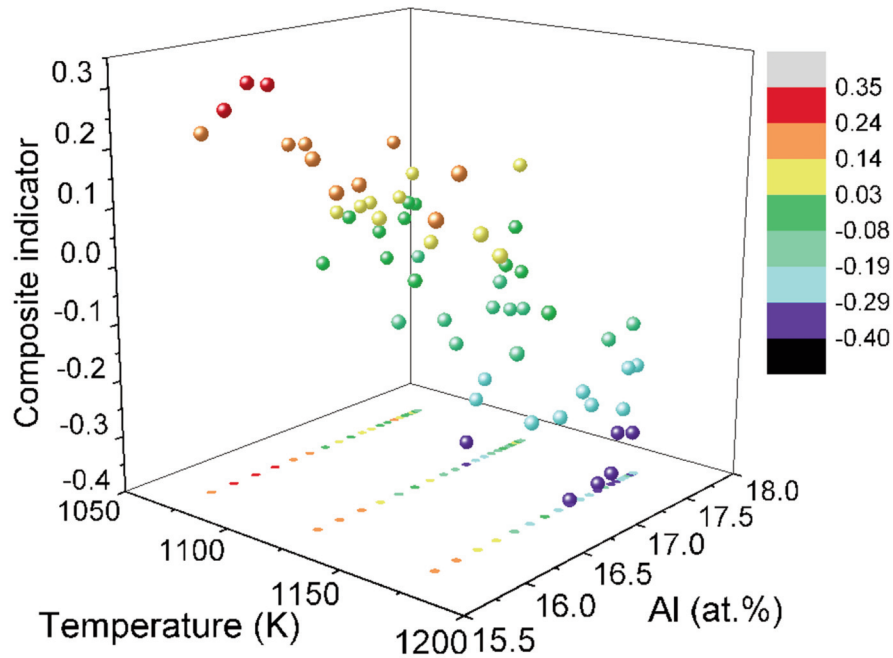


Figure 8. Evaluated composite indicators for binary Ni-Al alloys as a function of Al composition and aging temperature

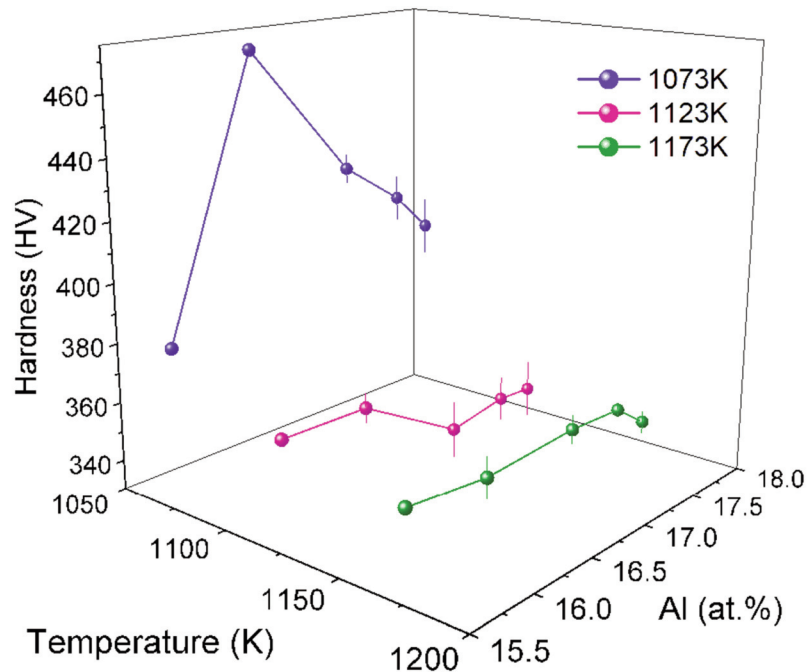


Figure 9. Measured hardness values of the Ni-13.4 at. % Al/Ni-17.4 at. % Al diffusion couples aging at 1,073 K, 1,123 K, and 1,173 K for 14,400 s

#### 4. Conclusion

Based on the prepared Ni-Al two-step diffusion couples, the effect of composition and aging temperature on the microstructure during aging, including the volume fraction, grain size, and shape

factor of  $\gamma'$  precipitates, as well as the hardness in  $\gamma+\gamma'$  two-phase region was comprehensively studied and analyzed.

By combining the microstructure information measured in this work and the previously proposed evaluation function of mechanical properties, the



optimal alloy composition and aging temperature for binary Ni-Al alloys with the best mechanical properties were efficiently screened to be Ni-16.2 at.% Al aging at 1073 K, which was then validated by the experimental hardness values.

The successful demonstration in binary Ni-Al system indicated that the two-step diffusion couple technique in combination with the evaluation function(s) for key properties could be used to perform the high-throughput screening of the optimal alloy composition and heat treatment process in the target alloys for the best mechanical properties.

### Acknowledgments

*The financial support from the projects of Key-Area Research and Development Programs of Guangdong Province (No.2019B010936001) and Guangzhou (No. 202007020008), the Guangdong Provincial Natural Science Foundation Project (No. 2020A1515010948), Special fund project of Guangdong Academy of Sciences (No:2020GDASYL-20200104028). Yijing Shang acknowledges the financial support from the Fundamental Research Funds for the Central Universities of Central South University (Grant No. 2019zzts938).*

### Reference

- [1] C.T. Sims, N.S. Stoloff, W.C. Hagel, *Superalloys II: High-Temperature Materials for Aerospace and Industrial Power*, Wiley-Blackwell, New York, 1987.
- [2] T.M. Pollock, S. Tin, *J. Propul. Power*, 22 (2) (2006) 361-347.
- [3] M.M. Barjesteh, S.M. Abbasi, K.Z. Madar, K. Shirvani, *J. Min. Metall. B*, 55 (2) (2019) 235-251.
- [4] P. Jozwik, M. Kopec, W. Polkowski, Z. Bojar, *J. Min. Metall. B*, 55 (1) (2019) 129-134.
- [5] H. Long, S. Mao, Y. Liu, Z. Zhang, X. Han, *J. Alloy. Compd.*, 743 (2018) 203-220.
- [6] J.Y. Chen, B. Zhao, Q. Feng, L.M. Cao, Z.Q. Sun, *Acta Metall. Sin.*, 46 (8) (2010) 897-906.
- [7] B.C. Wilson, J.A. Hickman, G.E. Fuchs, *JOM*, 55 (3) (2003) 35-40.
- [8] Y.Y. Qiu, *Acta Mater.*, 44 (12) (1996) 1969-4980.
- [9] M.V. Nathal, *Metall. Trans. A*, 18 (11) (1987) 1961-1970.
- [10] A.M. Ges, O. Fornaro, H.A. Palacio, *Mater. Sci. Eng. A*, 458 (1-2) (2007) 96-100.
- [11] H. Fu, S.S. Li, Y.L. Pei, S.K. Gong, *Mater. Sci. Forum*, 816 (2015) 297-303.
- [12] Y. Lin, G. Li, M. Wei, J. Gao, L. Zhang, *Metall. Mater. Trans. A*, 50 (10) (2019) 4920-4930.
- [13] D.J. Cao, N. Ta, L.J. Zhang, *Progress in Natural Science: Materials International*, 27 (6) (2017) 678-686.
- [14] N. Warnken, D. Ma, A. Drevermann, R.C. Reed, S.G. Fries, I. Steinbach, *Acta Mater.*, 57 (19) (2009) 5862-5875.
- [15] N. Ta, L.J. Zhang, Y. Du, *Metall. Mater. Trans. A*, 45 (4) (2014) 1787-1802.
- [16] R. Shi, D.P. Mcallister, N. Zhou, A.J. Detor, R. Didomizio, M.J. Mills, Y. Wang, *Acta Mater.*, 164 (2019) 220-236.
- [17] Y.H. Wen, B. Wang, J.P. Simmons, Y. Wang, *Acta Mater.*, 54 (8) (2006) 2087-2099.
- [18] J.C. Zhao, *Chin. Sci. Bull.*, 59 (15) (2014) 1652-1661.
- [19] J.C. Zhao, M.R. Jackson, L.A. Peluso, L.N. Brewer, *JOM*, 54 (7) (2002) 42-45.
- [20] J.C. Zhao, *J. Mater. Res.*, 16 (06) (2001) 1565-1578.
- [21] J.C. Zhao, *Methods for Phase Diagram Determination*, Elsevier Science Ltd, 2007, p.246-272.
- [22] S. Cao, J.C. Zhao, *J. Phase Equilib. Diffus.*, 37 (1) (2015) 25-38.
- [23] Q. Zhang, S.K. Makeneni, J.E. Allison, J.C. Zhao, *Scripta Mater.*, 160 (2019) 70-74.
- [24] T. Miyazaki, T. Koyama, S. Kobayashi, *Metall. Mater. Trans. A*, 30 (11) (1999) 2783-2789.
- [25] T. Miyazaki, *Prog. Mater. Sci.*, 57 (6) (2012) 1010-1060.
- [26] S. Mao, C. Wang, N. Li, J. Wang, Y. Chen, G. Xu, Y. Guo, Y. Cui, *Calphad*, 61 (2018) 219-226.
- [27] Y. Shang, S. Yang, L. Zhang, *Materialia*, 8 (2019) 100500.
- [28] L.J. Zhang, Y. Du, Q. Chen, I. Steinbach, B.Y. Huang, *Int. J. Mater. Res.*, 101 (12) (2010) 1461-1475.
- [29] W. Gust, M.B. Hintz, A. Loddwg, H. Odelius, B. Predel, *Phys. Status Solidi A*, 64 (1) (1981) 187-194.
- [30] D.H. Kirkwood, *Acta Metall.*, 18 (6) (1970) 563-570.
- [31] Y.Y. Qiu, *J. Alloy. Compd.*, 232 (1996) (1996) 254-263.
- [32] P. Cha, D. Yeon, S. Chung, *Scripta Mater.*, 52 (12) (2005) 1241-1245.
- [33] T. Grosdidier, A. Hazotte, A. Simon, *Mater. Sci. Eng. A*, 26 (1-2) (1998) 183-196.
- [34] A. Hazotte, T. Grosdidier, S. Denis, *Scripta Mater.*, 34 (4) (1996) 601-308.
- [35] J.X. Zhang, J.C. Wang, H. Harada, Y. Koizumi, *Acta Mater.*, 53 (17) (2005) 4623-4633.
- [36] Y.S. Yoo, *Scripta Mater.*, 53 (1) (2005) 81-85.
- [37] F. Binczyk, J. Śleziona, A. Kościelna, *Arch. Foundry Eng.*, 9 (3) (2009) 13-16.
- [38] A.B. Kamara, A.J. Ardell, C.N.J. Wagner, *Metall. Mater. Trans. A*, 27 (10) (1996) 2888-2896.
- [39] E.Y. Plotnikov, Z. Mao, R.D. Noebe, D.N. Seidman, *Scripta Mater.*, 70 (2014) 51-54.
- [40] Y.Y. Qiu, *J. Alloy. Compd.*, 270 (1-2) (1998) 145-153.
- [41] J.S. Van Sluytman, T.M. Pollock, *Acta Mater.*, 60 (4) (2012) 1771-1783.
- [42] M. Risbet, X. Feaugas, C. Guillemer-Neel, M. Clavel, *Mater. Charact.*, 59 (9) (2008) 1252-1257.



## PRIMENA DVOSTEPENE TEHNIKE DIFUZIONOG PARA TOKOM VISOKOPROPUSNOG SKRININGA OPTIMALNOG SASTAVA I TEMPERATURE STARENJA ZA DIZAJN LEGURA: PRIMER Ni-Al BINARNI SISTEM

Y.-J. Shang<sup>b</sup>, D.-J. Cao<sup>b</sup>, Q. Li<sup>b,\*</sup>, K. Yang<sup>a</sup>, C.-M. Deng<sup>a</sup>, L.-J. Zhang<sup>a,b,#</sup>

<sup>a</sup> Institut za nove materijale, Akademija nauka u Guandongu,  
Nacionalna inženjerska laboratorija za tehnologiju savremenih materijala,  
Glavna laboratorija u Guandongu za tehnologiju savremenih materijala, Guangdžou, Kina  
<sup>b</sup> Glavna državna laboratorija za metalurgiju praha, Centralnojužni univerzitet, Čangša, Hunan, Kina

### Apstrakt

Za potrebe ovog istraživanja su pripremljena četiri binarna Ni-13,4 at.% Al/Ni-17,7 at.% Al difuziona para koja su podvrgnuta homogenizaciji na 1573 K tokom 10800 s, nakon čega se formirao kontinuirani profil koncentracije. Tri difuziona para su nakon toga ohlađena radi starenja na odgovarajućim temperaturama, tj. na 1173, 1123 i 1073 K tokom 14400 s. Uticaj sastava i temperature starenja na mikrostrukturu starenja je detaljno proučen pomoću različitih eksperimentalnih tehnika i statističke analize. Zapreminski udeo, veličina zrna i faktor oblika  $\gamma'$  precipitata kod tri difuziona para su određeni u zavisnosti od sastava legure i temperature žarenja. Zajedno sa prethodno predloženom funkcijom evaluacije, u kojoj su za pokazatelje procene izabrani udeo faze, veličina zrna i faktor oblika  $\gamma'$  precipitata, određen je optimalni sastav legure i temperatura starenja za binarnu Ni-Al leguru sa najboljim mehaničkim svojstvima, što je konačno potvrđeno pomoću izmerenih vrednosti za tvrdoću. Uspešna demonstracija dizajna legure u takvoj binarnoj Ni-Al leguri ukazala je na činjenicu da bi dvostepeni difuzioni par, zajedno sa funkcijom procene mehaničkih svojstava, trebalo da predstavlja standard za visokopropusni skrining optimalnog sastava legure, kao i za postupak toplotne obrade kod drugih legura.

**Cljučne reči:** Dvostepeni difuzioni par; Ni-Al legura; Mikrostruktura; Tvrdoća; Dizajn legure

